

Ice templated nanocomposites containing rod-like hematite particles: Interplay between particle anisotropy and particle-matrix interactions

Cite as: J. Appl. Phys. **128**, 034702 (2020); <https://doi.org/10.1063/1.5144217>

Submitted: 07 January 2020 . Accepted: 28 June 2020 . Published Online: 17 July 2020

Guruswamy Kumaraswamy , Karthika Suresh , Hisay Lama, Madivala G. Basavaraj, and Dillip K. Satapathy 

COLLECTIONS

Paper published as part of the special topic on [Polymer-Grafted Nanoparticles](#)

Note: This paper is part of the Special Topic on Polymer-Grafted Nanoparticles.



View Online



Export Citation



CrossMark

ARTICLES YOU MAY BE INTERESTED IN

[Polymer-Grafted Nanoparticles](#)

Journal of Applied Physics **128**, 030401 (2020); <https://doi.org/10.1063/5.0019326>

[Two-dimensional gallium and indium oxides from global structure searching: Ferromagnetism and half metallicity via hole doping](#)

Journal of Applied Physics **128**, 034304 (2020); <https://doi.org/10.1063/5.0012103>

[Additive manufacturing and characterization of AgI and AgI-Al₂O₃ composite electrolytes for resistive switching devices](#)

Journal of Applied Physics **128**, 035103 (2020); <https://doi.org/10.1063/5.0004120>

Lock-in Amplifiers
up to 600 MHz



Ice templated nanocomposites containing rod-like hematite particles: Interplay between particle anisotropy and particle–matrix interactions

Cite as: J. Appl. Phys. 128, 034702 (2020); doi: 10.1063/1.5144217

Submitted: 7 January 2020 · Accepted: 28 June 2020 ·

Published Online: 17 July 2020



Guruswamy Kumaraswamy,^{1,a),b)}  Karthika Suresh,^{1,c)}  Hisayama,^{2,d)} Madivala G. Basavaraj,³
and Dillip K. Satapathy² 

AFFILIATIONS

¹Polymer Science and Engineering Division, CSIR—National Chemical Laboratory, Pune 411008, Maharashtra, India

²Soft Materials Laboratory, Department of Physics, Indian Institute of Technology Madras, Chennai 600036, Tamil Nadu, India

³Department of Chemical Engineering, Indian Institute of Technology Madras, Chennai 600036, Tamil Nadu, India

Note: This paper is part of the Special Topic on Polymer-Grafted Nanoparticles.

a) Author to whom correspondence should be addressed: guruswamy@iitb.ac.in

b) Current address: Department of Chemical Engineering, Indian Institute of Technology Bombay, Mumbai 400076, Maharashtra, India.

c) Current address: Department of Chemical Engineering and Materials Science, University of Minnesota, Twin Cities, Minneapolis, MN 55455-0431, USA.

d) Current address: Centre for Soft and Living Matter, Institute for Basic Science (IBS), Ulsan 44919, South Korea.

ABSTRACT

We demonstrate that the mechanical response of ice templated nanocomposite scaffolds prepared from ellipsoidal hematite particles is determined by both the particle aspect ratio and the interaction between the particles and the matrix polymer. We ice template aqueous dispersions of hematite particles, polyethyleneimine, and diepoxy crosslinker and crosslink the polymer in the frozen state. This protocol results in the formation of elastic macroporous monoliths capable of complete recovery from large compressive strains. Hematite particles show an inversion of their surface charge with pH: they are negatively charged at a basic pH and positively charged under acidic conditions. This allows us to change the interaction between hematite particles and crosslinked matrix polymer that they are embedded in, simply by immersing the monoliths in aqueous solutions with different pH's. We report that under basic conditions, viz, when polyethyleneimine adsorbs on the particle surface, there is a decrease in the monolith modulus with an increase in the particle aspect ratio. We demonstrate that this correlates with a change in the mechanism of monolith response: from wall compression for isotropic particles to wall bending for anisotropic particles with an aspect ratio of 4. Under acidic conditions (pH = 2), where hematite particles show a positive zeta potential, the monolith modulus increases with the aspect ratio of the ellipsoidal fillers. Understanding the interplay between filler aspect ratio and filler–matrix interaction has important implications for the control of nanocomposite mechanical properties.

Published under license by AIP Publishing. <https://doi.org/10.1063/1.5144217>

I. INTRODUCTION

In polymer nanocomposites, nanoparticle fillers are dispersed in a polymeric matrix with the objective of creating hybrid materials with synergistic properties.^{1–3} Typically, nanoparticle fillers are hard inorganics that impart rigidity and functional properties to the hybrid, while the polymeric matrix imparts toughness,

flexibility, and formability.^{4–8} In nanocomposites, the large specific area at the polymer/filler interface has important implications for the properties of the hybrid.^{9,10} Properties of polymer nanocomposites are strongly determined by polymer–filler interactions.^{11,12} In addition, filler–filler dispersed phase interactions, mediated by the continuous polymer matrix, also play an important role in

determining the properties of the hybrid. For example, when the fillers have an effective attractive interaction, the non-equilibrium dispersed morphology created by processing the nanocomposite evolves slowly, despite the high viscosity of the matrix polymer.^{13,14}

Of special interest are nanocomposites that incorporate anisotropic nanoparticles.¹⁵ For example, anisotropy reduces the percolation threshold of fillers in the matrix.¹⁶ Thus, conducting carbon nanotube composites can be prepared at ultralow concentrations of the nanotube inclusions.^{17,18} The aspect ratio of rod-like or plate-like fillers strongly influences the mechanical response of the hybrid nanocomposite. Researchers have reported an increase in the stiffness, strength, and heat distortion temperature with the increase in the aspect ratio of clays in nylon nanocomposites.¹⁹ In high inorganic content nacre-mimetic nanocomposites prepared using synthetic clays with different aspect ratios, an increase in stiffness and strength has been reported for higher aspect ratio clays.²⁰ In carbon nanotube nanocomposites, researchers have reported a qualitative change in the sign of the normal stress difference as a function of nanotube aspect ratio.^{21,22} They attribute this to a change in the nature of the network structures formed for the different aspect ratio nanotubes. Aggregation of nanofillers into network structures plays an important role in determining the effect of the nanofiller on the properties of the hybrid.²³ Therefore, the role of interparticle interactions in determining aggregation has been explored by several researchers.^{24,25} When filler interparticle interactions, or filler–matrix interactions can be tuned in response to changes in environmental conditions, then the nanocomposites are termed to be stimulus responsive. Recently, researchers have reported exciting advances in this area by synthesizing shape-memory materials²⁶ or biomimetic nanocomposite hydrogels capable of reversibly switching mechanical modulus by orders of magnitude in response to a stimulus.^{27,28}

Most of the experimental reports of filled polymers containing anisotropic nanoparticles have focused on high aspect ratio fillers, such as phyllosilicate clays, carbon nanotubes, or graphene. These nanocomposites typically contain only a few percent (by volume) of the fillers, since mechanical properties such as ductility deteriorate at higher filler loadings.²⁹ Polymer nanocomposites containing fillers with moderate anisotropy have not received attention in the literature. There are, however, reports that describe the packing of ellipsoidal particles. For example, Donev and co-workers have shown that ellipsoids show a non-trivial dependence of random packing volume fraction on particle aspect ratio, with a maximum for an aspect ratio less than 2.³⁰ They rationalize these results by showing that non-spherical particles have higher degrees of freedom, and require more nearest neighbors for mechanical stability. Jaeger and co-workers had shown that particle shape can change the modulus and yield stress of aggregates by about an order of magnitude for given confinement pressure.³¹ Basavaraj and co-workers have looked at the structural rearrangements of different aspect ratio particles in two-dimensional monolayers during compression.³² They observed that the compression modulus evolved non-monotonically with particle aspect ratio and that the modulus showed a maximum for an aspect ratio of 2.3. However, filler shape-dependence of the mechanical response of highly filled polymer nanocomposites has not been reported in the literature.

Our group has described the preparation of highly filled nanocomposites using ice templating, a facile process that employs an environmentally friendly solvent, water.³³ We have demonstrated the preparation of macroporous nanocomposites that show an impressive ability to recover completely from large compressive strains even at filler loadings as high as 90% by weight. Such materials have potential for use in a wide variety of applications ranging from biomedical scaffolds,³³ fire-retardant foams,³⁴ high-efficiency mixers in microfluidic devices,³⁵ or as flexible supercapacitors.³⁶ Recently, we have explored the microstructural origins of the remarkable mechanical response of such ice templated monoliths in detail.^{37–39} Our studies demonstrate that the mechanical response of the monoliths is dominated by a thin [$\sim O(10\text{ nm})$] mesh of a crosslinked polymer that holds the filler particles in the monolith. The structure of the polymer that forms this mesh is critically determined by the processing conditions employed during monolith synthesis. Therefore, the mechanical response of the monolith is highly sensitive to the protocol for monolith synthesis. Recently, we have demonstrated the effect of changing filler–polymer interactions in preformed monolith.⁴⁰ This was possible by immersing the monoliths in aqueous solutions at different pH's. For monoliths prepared using approximately spherical fillers, we reported that weakening the attractive interactions between the crosslinked polymer mesh and the embedded fillers resulted in a decrease in the monolith modulus.⁴⁰

Ice templated nanocomposite hybrids that incorporate anisotropic nanoparticles and that are prepared using the protocol described by Rajamanickam *et al.*³³ have not been reported. Here, we describe the formation of ice-templated macroporous nanocomposites prepared using ellipsoidal hematite particles with an aspect ratio varying from ≈ 1 to ≈ 4 . The surface charge of these hematite particles can be changed from positive to negative simply by varying the pH. Immersing the macroporous monolith sponges in aqueous solutions at different pH's allows us to systematically vary the interactions between the polymer matrix and the hematite particles embedded in it. Here, we explore the effect of particle aspect ratio and particle–matrix interactions on the mechanical response of nanocomposite hybrid monoliths and relate the mechanical properties to the monolith structure.

II. EXPERIMENTAL DETAILS

A. Materials

Polyethyleneimine (PEI, 25 kg/mol), 1,4-butanediol diglycidyl ether, acetic acid, sodium hydroxide (NaOH), and $\text{Fe}(\text{ClO}_4)_3$ were sourced from Sigma Aldrich and were used without any further purification. Urea and NaH_2PO_4 were obtained from Merck, India, and were used as received.

B. Preparation of ellipsoidal hematite particles and their ice templated scaffolds

Anisotropic hematite particles were synthesized by the hydrolysis of Fe^{+3} using methods previously reported in the literature.⁴¹ This synthesis results in the formation of ellipsoidal particles, whose aspect ratio can be systematically varied by adjusting the concentration of NaH_2PO_4 added to the reaction mixture. In a

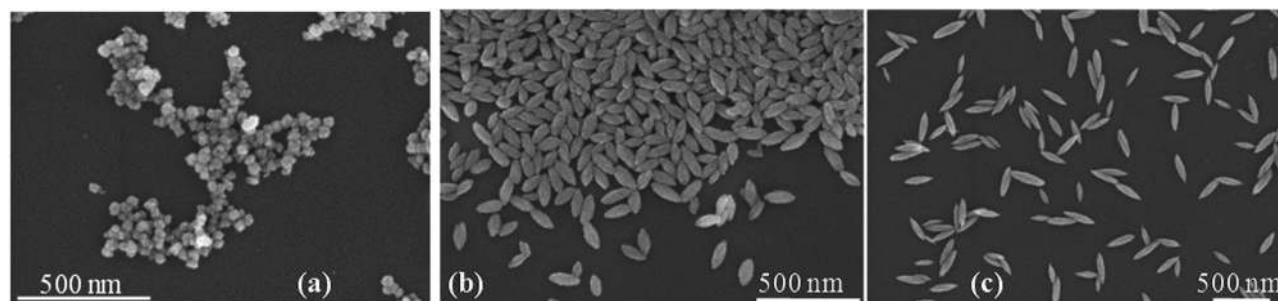


FIG. 1. Scanning electron microscopy of hematite particles with aspect ratios (a) ~ 1 , (b) ~ 2.2 and (c) ~ 4 .

typical preparation, 3.54 g of $\text{Fe}(\text{ClO}_4)_3$, 0.6 g of urea, and a controlled amount of NaH_2PO_4 were added to 100 ml of Milli-Q water in a clean 250 ml Pyrex bottle. The Pyrex bottle is kept in a preheated oven at 100 °C for 24 h. Subsequently, the reaction product is separated by centrifugation and is repeatedly washed with de-ionized distilled (DD) water until the pH of the supernatant is neutral. The washed product is dispersed in DD water. We confirm the structure of the hematite nanoparticles synthesized using x-ray diffraction (supplementary material, Fig. S1). The shape and size of the hematite particles are characterized using SEM (Hitachi S-4800, Japan). In this work, we prepare hematite particles that are approximately isotropic (viz, aspect ratio = 1) as well as ellipsoids with aspect ratios (=length/maximum diameter, viz, L/D) of 2.2 and 4, as shown in Fig. 1 and Table I.

We now describe the preparation of a typical ice-templated scaffold. Hematite dispersions (688 μl) containing 60 mg by weight of the particles were added to 80 μl of PEI stock solution (10 wt. %) and vigorously mixed for about 10 min using a vortex mixer. Next, 8 mg of 1,4-butanediol diglycidyl ether was added to this dispersion and vortexed for about 3 min, and were then immediately transferred to the refrigerator. To prepare ice-templated scaffolds, we followed the protocol described in our previous publications.^{33,40} Briefly, the pH of the dispersions were maintained at 10, and the dispersions were frozen in centrifuge tubes by placing them in a freezer at -18°C . They were held at this temperature for 24 h, during which time PEI is crosslinked through the diepoxo to form a network. Subsequently, the samples were freeze dried (Labconco FreeZone 2.5 Plus, -80°C , 0.1 mbar). Thus, the dry scaffold is a macroporous material whose walls are comprised of hematite particles 79% by weight [= 60/(60 + 8 + 8)] enmeshed in a crosslinked PEI matrix. A schematic representation of the process for preparation of ice-templated scaffolds is depicted in Fig. 2.

TABLE I. Dimensions and aspect ratio of hematite particles obtained from scanning electron micrographs.

Particle label	Length (nm)	Diameter (nm)	Aspect ratio
1		105 ± 12	~ 1
2.2	119 ± 10	53 ± 3	2.2
4	196 ± 6	49 ± 2	4.0

C. Methods

To visualize the microstructure of the scaffold, we have performed scanning electron microscopy (SEM) on a slice of the lyophilized sample (scaffold) using FESEM, INSPECT F50 (UK). Prior to SEM imaging, a slice of the lyophilized sample was placed on a copper tape and mounted on the SEM specimen stub and then sputter-coated with gold. Coating of gold on the sample enhances its electrical conductivity and improves the quality of SEM images. The SEM images of the scaffolds displaying the local microstructure comprising of particles having aspect ratios of 1, 2.2, and 4 are shown in Figs. 2(a)–2(f).

Mechanical properties of the monolithic sponges were measured using an ARES-G2 rheometer (TA Instruments). The rheometer is equipped with a force rebalance torque transducer and is capable of making normal force measurements. Cylindrical hydrogel monolith samples were measured using the 8 mm diameter plate-plate geometry. To avoid sample slippage during measurements, roughened parallel plates were used. Care was taken to ensure proper contact between the sample and measuring plates. Samples were placed on the bottom plate and the top plate was moved to contact the top of the sample until a normal force of 1 g was measured. Small amplitude oscillatory measurements were performed to measure the shear moduli. The samples were also compressed (and then allowed to re-expand) in the rheometer and the normal forces exerted were measured. All measurements were repeated at least three times on fresh samples to confirm their reproducibility. Representative data are presented in this work.

The nominal density of the monoliths was measured by taking a cylindrical sample and by carefully measuring its mass (using a weighing balance with an accuracy of 0.1 mg) and dimensions (using a micrometer with an accuracy of 1 μm). The zeta potential of particles at different pH's was obtained from electrophoretic mobility of particles measured using Zeta PALS (Brookhaven Instruments Corp., Holtsville, NY, USA). The pH of dilute particle dispersions was adjusted by the addition of acetic acid or NaOH solutions of known concentration.

III. RESULTS AND DISCUSSION

Ice templating results in the formation of a monolithic nanocomposite. During ice templating, we freeze dispersions whose pH

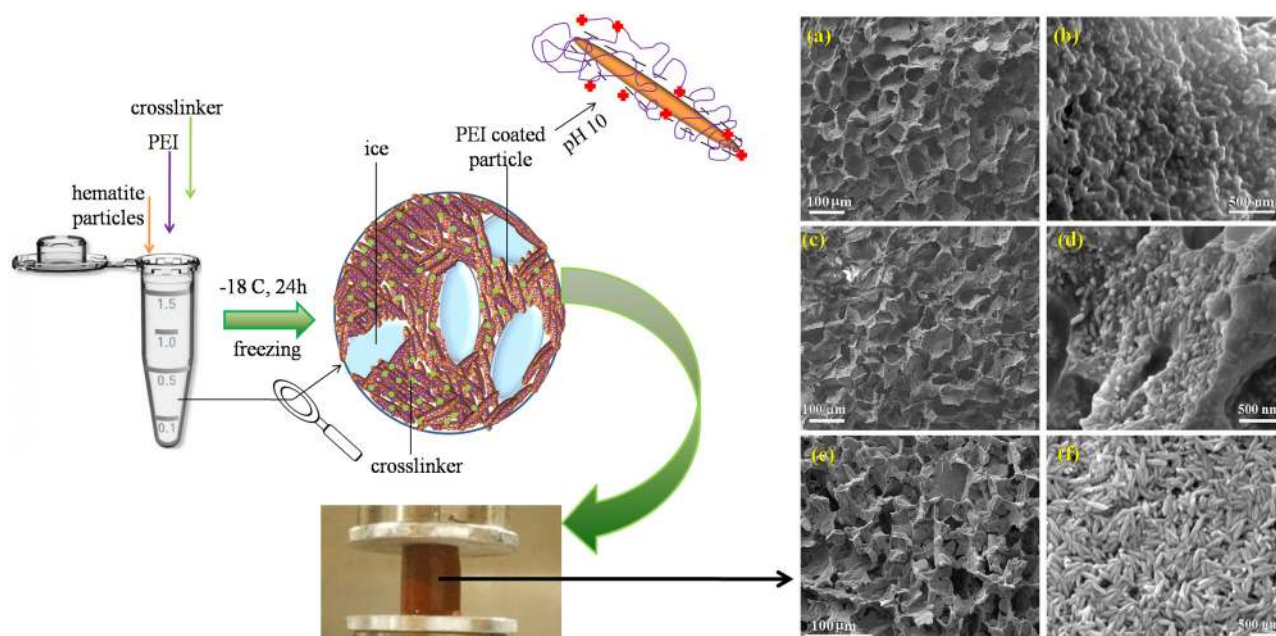


FIG. 2. Schematic of scaffold preparation protocol and the scanning electron micrographs of scaffolds made of hematite particle with aspect ratios (a) and (b) ~ 1 , (c) and (d) ~ 2.2 , and (e) and (f) ~ 4 . (b), (d), and (f) are the high resolution SEM images of pore walls.

is adjusted to 10. At this pH, hematite particles are negatively charged and cationic PEI adsorbs on their surface due to electrostatic interactions. Hematite particles, PEI, and diepoxy crosslinker are consolidated by the growing ice crystals and form the walls of pores in the monolith. The reaction between PEI and diepoxy crosslinker is very slow at room temperature, at the concentrations employed in the monolith preparation. However, due to the local increase in concentration on freezing, PEI reacts with diepoxy crosslinker even at the temperatures in the refrigerator ($\sim -18^\circ\text{C}$). We allow the reaction to proceed for a day. Subsequently, the samples are freeze dried to yield a macroporous monolith with a volume porosity about 90%. The monoliths take the shape of the centrifuge tube in which they are prepared—therefore, they are cylindrical in shape with a diameter of 8 mm and a length of about 1 cm (Fig. 2). The aspect ratio of the hematite particles does not influence ice crystal formation and similar pore size distributions are obtained for monoliths prepared using the different particles. In all cases, an analysis of the SEM images (Fig. 2) suggests that pore sizes vary from 30 to 130 microns, with the pore size distribution peaking at about $60\ \mu\text{m}$. High resolution SEM images of the pore walls [Figs. 2(b)–2(f)] reveal the presence of hematite particles embedded in them. Even as the aspect ratio of the particles increases from 1 to 2.2 to 4, we do not observe any orientational order for the particles in the pore walls (supplementary material, Fig. S2). We estimate a Peclet number based on the rate of growth of ice crystals as $Pe = v/D_R L$, where v is the rate of propagation of the freezing front (estimated as $100\ \text{nm/s}$),⁴² D_R is the rotation diffusion coefficient,⁴³ and L is the length of the particle. We calculate

$Pe \ll 1$, suggesting that particles consolidated into walls during ice templating should show orientational correlations. However, it appears that the process of ice templating consolidates particles in such a way that even anisotropic ellipsoidal particles with an aspect ratio of 4 are unable to align. We believe that this might be due to short range attractive interactions between hematite particles due to the possibility of PEI chains forming bridges between them. We reason that these sticky interactions between ellipsoids preclude their orientation. Our previous studies indicate that macropore walls formed by ice-templating comprise particles enmeshed in a network of crosslinked PEI.^{38,40} As a consequence of this structure, monoliths recover completely after large compressive deformations, exceeding strains of 70%. All the hematite monoliths investigated in this work are elastic and show recovery after large compressive deformations.

We use dynamic oscillatory shear rheology to probe the shear response of monoliths containing different aspect ratio hematite ellipsoids (Fig. 3). Monoliths are soaked in water, and sodium hydroxide is added to maintain $\text{pH} = 10$. Thus, these are nanocomposite hydrogels. Monoliths prepared using different aspect ratio hematite show qualitatively similar frequency dependence for their mechanical response. As would be expected for a network material, the elastic modulus, G' , is significantly higher (by about an order of magnitude) than the loss modulus, G'' . The elastic modulus shows a very weak frequency dependence, $G' \sim \omega^x$, where $x \sim O(10^{-2})$, for all monoliths. The monoliths are remarkably soft, with G' between about 4000 and 10 000 Pa, comparable to the elastic modulus of macroporous monoliths of unfilled crosslinked PEI

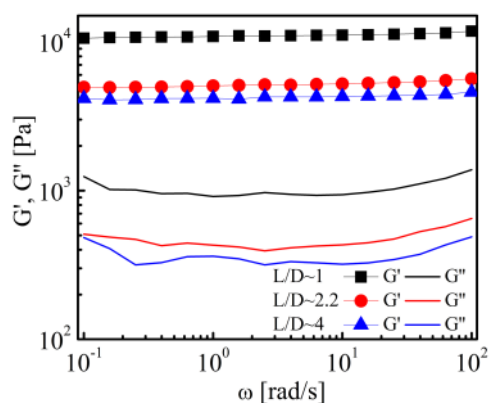


FIG. 3. Storage (G') and loss (G'') moduli at pH = 10 as a function of frequency for scaffolds made with different aspect ratio hematite particles.

(supplementary material, Fig. S3). This suggests that the mechanical response arises primarily from the network of crosslinked polymer and not directly from the filler particles. We reiterate that the hematite weight fraction for all monoliths is identical, to within the experimental error.

We observe that G' decreases with an increase in the hematite aspect ratio. This decrease in modulus with increase in filler aspect ratio is qualitatively different from the trends reported in the literature. In nanocomposites comprising silica nanoparticles with aspect ratio varying from 1 to 10 in an SBR rubber, Scotti and co-workers reported an increase in the modulus with filler aspect ratio.^{44,45} They attributed this to improved percolation for higher aspect ratio fillers. Their results are consistent with those reported for nanocomposites containing very high aspect ratio nanofillers, including rod-like carbon nanotubes²³ and plate-like clay particles.^{19,46} In all these, an increase in filler aspect ratio resulted in increased modulus, attributed to increased filler–filler interactions with increase in the filler aspect ratio. Therefore, the decrease in

modulus with hematite aspect ratio observed in our experiments (Fig. 3) is unusual. We note that in the case of polymer nanocomposites containing moderate aspect ratio silica particles or high aspect ratio clay or CNTs (where the modulus increases for particles with increased aspect ratio), the particle matrix interaction is not characterized by strong attraction. Even when the clay or CNT is compatibilized by surface treatment so that mixing and dispersion can be achieved, typically, one does not observe strong attraction between the matrix and the filler in the nanocomposites. Furthermore, while highly filled nanocomposites have been reported, the filler concentration is typically much lower than for the case of the ice-templated monoliths reported in this work. It is possible that these differences contribute to the unusual aspect ratio dependence of the modulus that we observe for ice templated scaffolds.

To further investigate the origins of the unusual dependence of the mechanical response on hematite aspect ratio, we examine the variation in monolith modulus with its nominal density. For this, we prepare monoliths by ice templating dispersions with different concentrations (while maintaining the ratio of particle to polymer to crosslinker). Thus, all monoliths have the same hematite weight fraction ($\approx 79\%$). For lower dispersion concentrations, the volume occupied by the macropore walls is a smaller fraction of the monolith volume resulting in a lower nominal density (ρ^*) for the monolith. Note that the walls are dense, comprising hematite particles in a polymer mesh and there is likely no variation in the density within the walls for these monoliths. The protocol employed for ice templating is the same for all monoliths. We observe that monoliths containing isotropic hematite exhibit an approximately linear dependence of modulus with nominal density, viz, $G' \sim \rho^*$ [Fig. 4(a)]. Furthermore, we observe that Young's modulus, E' , obtained from the linear region of the stress–strain curve for compression also scales as $\sim \rho^*$ [Fig. 4(a)]. We note that $E' \approx 2G'$, indicating that the Poisson ratio, $\nu \approx 0$. Consistent with this, we note that there is no change in the lateral dimension of the monoliths when they are compressed. These results are in accordance with our previous reports for ice templated monoliths of

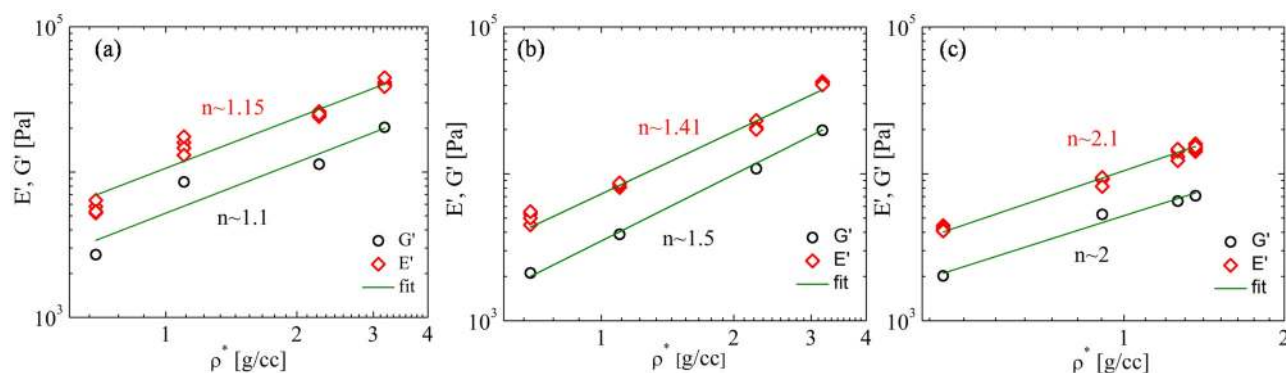


FIG. 4. Storage and Young's moduli as a function of scaffold nominal density (ρ^*) for scaffolds made of hematite particles with aspect ratios (a) ~ 1 , (b) ~ 2.2 , and (c) 4. Note that measurements for Young's modulus are repeated four times and data from all the measurements are presented. All data are at pH = 10. The lines shown are power law fits to the data with exponent n .

approximately spherical silica particles.^{33,47} We observe a systematic transition in the nominal density dependence of the modulus with increase in aspect ratio of the hematite particles. For ellipsoids with an aspect ratio of 2.2 and 4, we observe $G', E' \sim \rho^{*1.5}$ and $G', E' \sim \rho^{*2}$, respectively. For these scaffolds as well, $E' \approx 2G'$. We note that G' and E' are independent quantities—therefore, given that we can access only a relatively small range of ρ^* , it is reassuring that both moduli show similar scaling behavior.

We interpret this difference in ρ^* scaling as arising from a change in the mechanism of monolith response. The dimensions of the hematite particles are of the order of $\sim O(100 \text{ nm})$, orders of magnitude smaller than the size of one cell in the monolith (of the order of $100 \mu\text{m}$). The samples on which we perform mechanical measurements are macroscopic (of the order of 1 cm), orders of magnitude larger than the size of the porous cells in the monolith. Therefore, it is reasonable to consider the samples as isotropic materials amenable to a continuum description. We consider two independent modes by which the monolith responds to mechanical deformation, following standard descriptions⁴⁸ of three-dimensional foams.

If the compressive response of the foam arises from compression of the cell walls, then the work done by the compressive force, F , during deformation can be written as $F\delta = E_W d^2 t \epsilon^2$, where δ is the change in pore dimension along the compression axis, E_W is the modulus of the pore wall, d is the pore diameter, t is the wall thickness, and ϵ is the nominal strain ($=\delta/d$). Based on this, the experimentally observed nominal modulus of the foam can be written as $E = (\text{nominal stress})/\text{strain} = (F/d^2)/(\delta/d)$. Therefore, $E'\delta^2 \sim E_W d^2 t (\delta^2/d^2)$, leading to

$$E'/E_W \sim t/d. \quad (1)$$

If the density of the pore walls is ρ_W , then we can write $\rho_W(d^2 t) \sim \rho^* d^3$. Thus, $\rho^*/\rho_W \sim t/d$ and Eq. (1) can be written as

$$E'/E_W \sim t/d \sim \rho^*/\rho_W. \quad (2)$$

Thus, $E' \sim \rho^*$ (and $G' \sim \rho^*$) as is observed for ice templated monoliths prepared using isotropic particles. This suggests that the origin of the mechanical response when the monolith is deformed is compression of the walls.³³ This is in itself unusual—typically, open cell monoliths respond through bending of the cell walls rather than by wall compression. When monoliths respond by bending of cell walls, beam theory for linear elastic deflection shows that the deflection, $\delta \sim Fd^3/E_W I$, where I is the second moment of the area of the cell wall. Therefore, Young's modulus is given as $E' = \sigma/\epsilon \sim E_W I/d^4$. Thus, we obtain

$$E'/E_W \sim (\rho^*/\rho_W)^2. \quad (3)$$

Thus, $E', G' \sim \rho^{*2}$ as is observed for ice templated monoliths prepared using ellipsoidal particles with aspect ratio = 4. This suggests that ice templated monoliths using ellipsoidal particles with aspect ratio = 4 respond to deformation by bending of cell walls. We note that there is a systematic increase in the ρ^* dependence of G' as aspect ratio is increased from ≈ 1 to ≈ 4 , suggestive of a change from cell wall compression to bending in response to

deformation of the monolith. The mechanical response of the monoliths arises from the polymer shells—ice templated monoliths are soft and we have previously demonstrated that their modulus increases linearly with temperature, pointing to the polymeric contribution to their response.³³ Therefore, when a monolith is compressed and there is relative motion between the particles in the wall, the response of the monolith arises from how the crosslinked polymer mesh that holds the particles together is deformed to accommodate this relative motion. It appears that for the case of isotropic particles, the preferred mode is for particles to move relative to each other so that the wall gets compressed rather than bend, while for higher aspect ratio ellipsoids, it is easier for the particles to slide relative to each other rather than change the interparticle spacing, so that the walls bend rather than get compressed. Thus, the decrease in E, G' with the increase in particle aspect ratio appears to correlate with a change in the mechanism of monolith response.

The surface charge of hematite particles is a strong function of pH. At low pH, viz, under acidic conditions, the particles are positively charged, with a zeta potential above $+50 \text{ mV}$ at $\text{pH} = 2$. The particle charge decreases with an increase in pH and the particles are nearly uncharged at a neutral pH. Under basic conditions, the particles bear a negative surface charge (zeta potential = -40 mV at $\text{pH} = 10$) (Fig. 5). We note that monoliths are always prepared from basic aqueous dispersions. Here, PEI chains adsorb on the negatively charged hematite particles and, the reaction between the PEI amine groups and the diepoxy groups can proceed. However, once the crosslinking reaction is complete and the ice templated monoliths have been prepared, the walls comprise hematite particles trapped in a crosslinked mesh of PEI. These monoliths can be dried and soaked in aqueous solutions at different pH values so that we can qualitatively change the interactions between the embedded hematite particles and the crosslinked polymer matrix. We now examine the response of monoliths as hydrogels, immersed in water at different pH ranging from 2 to 10. At the outset, we comment that the pH dependence of the monolith response is a consequence of the change in the zeta potential of the hematite particles. We have shown previously that “control”

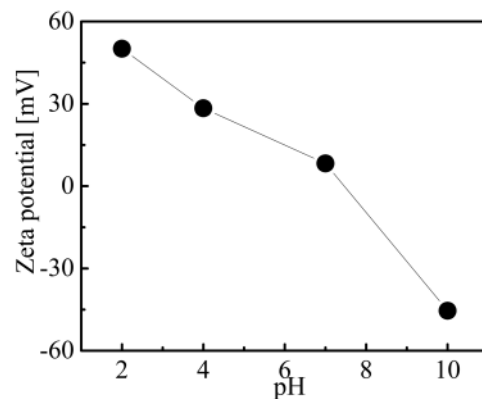


FIG. 5. Zeta potential measurements of hematite particles as a function of pH.

unfilled monoliths prepared by crosslinking ice templated PEI solutions do not exhibit any pH dependence to their mechanical properties.⁴⁰ A change in pH results in a change in the zeta potential of the hematite particles and therefore, possibly in changes to the hematite–hematite and hematite–polymer matrix interactions in the monoliths.

At pH = 10, there are attractive interactions between the matrix crosslinked PEI and the embedded hematite fillers. At neutral or acidic pH, the zeta potential of dispersed hematite particles varies from near 0 to positive. Under these conditions, PEI will not adsorb on the particle surface. In fact, zeta potential measurements indicate that PEI chains adsorbed on hematite particle surfaces desorb when the pH is decreased from basic to acidic values. Therefore, when monoliths are soaked in water maintained at neutral to acidic pH, we anticipate that the matrix polymer interaction will transform from attractive to repulsive. However, since the hematite particles in the monoliths are trapped in a crosslinked PEI mesh, they cannot escape from the matrix or aggregate in the matrix, even if the matrix-particle interaction turns repulsive. For monoliths prepared using isotropic silica particles, we had demonstrated that repulsive matrix-filler interactions results in a decrease in G' .⁴⁰

Monoliths prepared with hematite particles with different aspect ratios (but with same ρ^*) exhibit qualitatively different pH dependence of the modulus. Isotropic hematite monoliths show a decrease in G' as pH decreases from 10 to 2. As the aspect ratio is increased to ≈ 2.2 , we observe that G' exhibits almost no pH dependence (Fig. 6). For monoliths prepared using the high aspect ratio (≈ 4) hematite, we observe that G' decreases as pH increases from acidic (pH = 2) to neutral to basic (pH = 10) (Fig. 6). At pH = 2, the aspect ratio dependence of G' is exactly opposite to the trend at pH = 10, viz, G' increases with the aspect ratio of the ellipsoidal hematite particles (Fig. 6).

Qualitative differences between the behavior at pH = 2 and = 10 are also observed in large amplitude compression experiments on monoliths containing the hematite particles. We subject monoliths prepared using hematite particles with different aspect

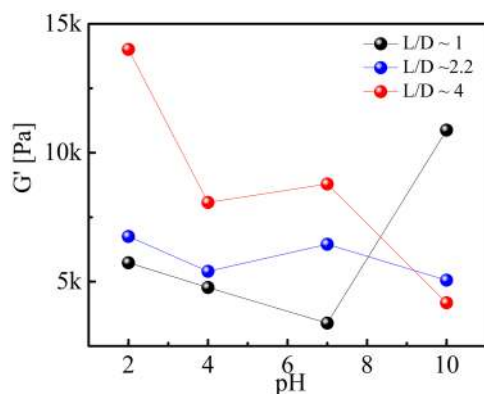


FIG. 6. Storage modulus (at 1 rad/s) as a function of pH for same density scaffolds made with different aspect ratio (L/D) hematite particles.

ratio, and soaked in water at different pH's to compressive strain followed by unloading. We observe that all monoliths are elastic and recover from 70% compressional strain at pH from 2 to 10 (Fig. 7). In all our experiments, the monoliths exhibit a linear response region where compressional stress is proportional to strain. Subsequently, the stress increases monotonically but at a lower rate until about a strain of 40%. Beyond that, there is a sharp increase in stress with increasing strain. Since the Poisson ratio for the ice templated monoliths is nearly 0, there is a decrease in the void volume as the monoliths are compressed. We have previously demonstrated that beyond about 40% strain, the cell walls collapse and the pore walls come into contact.⁴⁷ Therefore, the sharp increase in stress can be attributed to the compression of a dense monolith as the void volume is eliminated due to compression. After compression to 70% strain, the monoliths are unloaded and there is a decrease in stress. As previously reported, here too we observe a hysteresis in the stress–strain response. The area corresponding to the hysteresis loop is approximately 30%, largely independent of the aspect ratio of the hematite ellipsoids and the pH at which the experiment is carried out. A change in pH from 2 to 10 results in the hematite/PEI matrix interaction changing from repulsive to attractive. Thus, it appears that hysteresis in the stress–strain response does not result from interactions at the particle–polymer interface. We believe that the hysteresis arises from viscous dissipation in the crosslinked polymer matrix. We note that compression–recovery cycles on pure polymer monoliths (containing no filler particles) also show hysteresis (Supporting Information, Figure S3), supporting our contention that hysteresis arises from viscous dissipation in the polymer matrix. The Young's modulus, E' , calculated from the low strain linear response region during compression and, σ_m , the maximum stress at 70% compression are both higher for aspect ratio = 4 ellipsoidal particles relative to isotropic particles for pH = 2 while the trend is opposite for pH = 10 (Fig. 7). The values for the modulus, E' and maximum stress, σ_m do not change monotonically as a function of pH from 2 to 10. There is significant variability in the data measured at pH = 7, possibly since this is close to the isoelectric point for the hematite particles. Therefore, we focus on the trends observed for experiments conducted at the two extreme values of pH (= 2 and = 10).

At pH = 2, hematite particles in dispersion have a positive surface charge. Zeta potential measurements indicate that PEI chains adsorbed on hematite particles at pH = 10 desorb off the particle surface when the pH is changed to 2 by the addition of acid. Therefore, at pH = 2, we anticipate that the interaction between the hematite particle surface and crosslinked PEI mesh that surrounds it is repulsive. This repulsive interaction leads to a reduction in the number of PEI/hematite contacts relative to the attractive case. Again, we reiterate that since the monolith comprises hematite particles in a crosslinked PEI mesh, the particles cannot escape the mesh or aggregate in it, even at pH = 2. At pH = 2, there is an increase in the modulus (G' and E') and in σ_m with increase in aspect ratio, as has been reported for polymer–silica nanocomposites (with moderate aspect ratio silica fillers)^{44,45} as well as polymer–clay and CNT–polymer nanocomposites.^{19,23,46} Those systems too are characterized by incompatibility between the filler and the matrix polymer. Typically, the filler surfaces are treated so that they are rendered compatible with the matrix

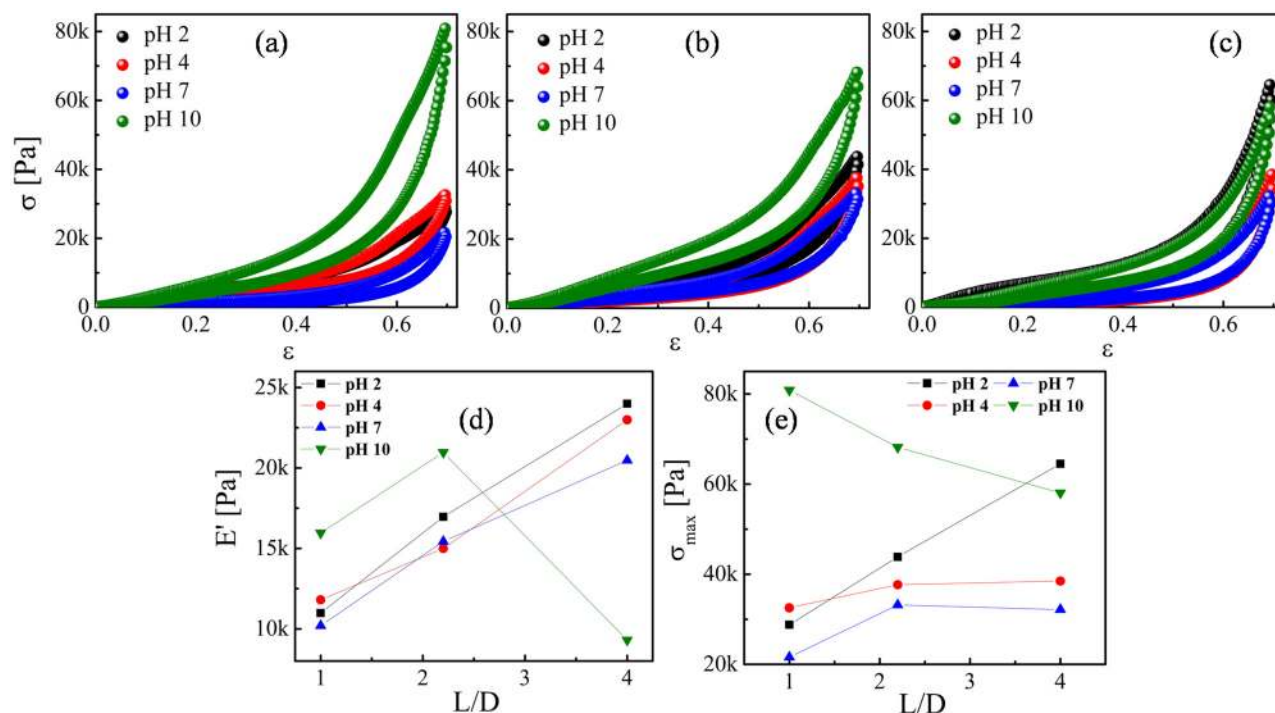


FIG. 7. Mechanical properties of scaffold at different pH. Compression–expansion curves at 70% strain of scaffolds made of particles with aspect ratios (a) ~ 1 , (b) ~ 2.2 , and (c) ~ 4 . (d) and (e) are Young's moduli vs aspect ratio and maximum compressive stress (σ_{max}) at 70% strain vs aspect ratio, respectively.

polymer. However, achieving good filler dispersion in a polymer matrix for clay or CNT nanocomposites remains challenging. In our system, where we can change filler–polymer interactions by changing pH, we note that for systems where there are strong attractive interactions between filler and polymer, an increase in filler aspect ratio correlates with a change in the mechanical response and with a decrease in modulus. In contrast, when there are repulsive interactions between the filler and polymer, the modulus increases with aspect ratio. At this point, there is insufficient data in the literature to state that this is a general observation. However, this interesting observation based on our results suggests a potentially interesting line of future investigation.

IV. CONCLUSIONS

The mechanical response of ice templated monolith hydrogels comprising ellipsoidal hematite particles in a crosslinked PEI matrix depend on the aspect ratio of the particles and the pH at which the measurement is performed. The ice templated monoliths recover elastically after being subjected to large compressive strains, of up to 70%, independent of the aspect ratio of the hematite particle and the pH at which they are compressed. Under acidic conditions (pH = 2), there is a repulsive interaction between the particle surface and the crosslinked polymer matrix. Under these conditions, we observe an increase in the monolith modulus with aspect

ratio. Monolith response at pH = 10, where there is an attractive interaction between the particle and polymeric matrix show a qualitative different response. Here, the monolith modulus decreases with increase in aspect ratio. At pH = 10, the monolith modulus increases approximately linearly with nominal density for isotropic particles. As the particle aspect ratio increases, there is a systematic increase in the density dependence of the modulus. Our results suggest that the mechanical response of ice templated monolith hydrogels depend on both the aspect ratio of the particles in the nanocomposite and on the nature of the particle–matrix interactions.

SUPPLEMENTARY MATERIAL

See the [supplementary material](#) for the characterization of the hematite particles (XRD), characterization of the monoliths (SEM) indicating local ordering of the colloidal particles and mechanical characterization of ice templated monoliths of neat crosslinked polymer.

ACKNOWLEDGMENTS

K.S. acknowledges CSIR for the GATE fellowship. G.K. acknowledges BRNS for partial funding of this research.

DATA AVAILABILITY

The data that support the findings of this study are available from the corresponding author upon reasonable request.

REFERENCES

- ¹S. S. Ray and M. Okamoto, *Prog. Polym. Sci.* **28**(11), 1539 (2003).
- ²S. K. Kumar and R. Krishnamoorti, *Annu. Rev. Chem. Biomol. Eng.* **1**, 37 (2010).
- ³K. I. Winey and R. A. Vaia, *MRS Bull.* **32**(4), 314 (2007).
- ⁴A. B. Morgan, *Polym. Adv. Technol.* **17**(4), 206 (2006).
- ⁵G. Choudalakis and A. D. Gotsis, *Eur. Polym. J.* **45**(4), 967 (2009).
- ⁶Y. Zhang, S. Gong, Q. Zhang, P. Ming, S. Wan, J. Peng, L. Jiang, and Q. Cheng, *Chem. Soc. Rev.* **45**(9), 2378 (2016).
- ⁷A. J. Crosby and J. Y. Lee, *Polym. Rev.* **47**(2), 217 (2007).
- ⁸V. K. Thakur and M. R. Kessler, *Polymer* **69**, 369 (2015).
- ⁹L. S. Schadler, S. K. Kumar, B. C. Benicewicz, S. L. Lewis, and S. E. Harton, *MRS Bull.* **32**(4), 335 (2007).
- ¹⁰A. Bansal, H. Yang, C. Li, K. Cho, B. C. Benicewicz, S. K. Kumar, and L. S. Schadler, *Nat. Mater.* **4**(9), 693 (2005).
- ¹¹R. A. Vaia, K. D. Jandt, E. J. Kramer, and E. P. Giannelis, *Chem. Mater.* **8**(11), 2628 (1996).
- ¹²P. Reichert, H. R. Nitz, S. Klinke, R. Brandsch, R. Thomann, and R. Mulhaupt, *Macromol. Mater. Eng.* **275**(1), 8 (2000). [https://doi.org/10.1002/\(SICI\)1439-2054\(20000201\)275:1<8::AID-MAMES>3.0.CO;2-6](https://doi.org/10.1002/(SICI)1439-2054(20000201)275:1<8::AID-MAMES>3.0.CO;2-6)
- ¹³G. Galgali, C. Ramesh, and A. Lele, *Macromolecules* **34**(4), 852 (2001).
- ¹⁴G. P. Baeza, C. Dessi, S. Costanzo, D. Zhao, S. Gong, A. Alegria, R. H. Colby, M. Rubinstein, D. Vlassopoulos, and S. K. Kumar, *Nat. Commun.* **7**, 11368 (2016).
- ¹⁵H. Kim, A. A. Abdala, and C. W. Macosko, *Macromolecules* **43**(16), 6515 (2010).
- ¹⁶J. Li and J.-K. Kim, *Compos. Sci. Technol.* **67**(10), 2114 (2007).
- ¹⁷W. Bauhofer and J. Z. Kovacs, *Compos. Sci. Technol.* **69**(10), 1486 (2009).
- ¹⁸J. K. W. Sandler, J. E. Kirk, I. A. Kinloch, M. S. P. Shaffer, and A. H. Windle, *Polymer* **44**(19), 5893 (2003).
- ¹⁹J. I. Weon and H. J. Sue, *Polymer* **46**(17), 6325 (2005).
- ²⁰P. Das, J.-M. Malho, K. Rahimi, F. H. Schacher, B. Wang, D. E. Demco, and A. Walther, *Nat. Commun.* **6**, 5967 (2015).
- ²¹S. B. Kharchenko, J. F. Douglas, J. Obrzut, E. A. Grulke, and K. B. Migler, *Nat. Mater.* **3**(8), 564 (2004).
- ²²D.-H. Xu, Z.-G. Wang, and J. F. Douglas, *Macromolecules* **41**(3), 815 (2008).
- ²³A. Martone, G. Faiella, V. Antonucci, M. Giordano, and M. Zarrelli, *Compos. Sci. Technol.* **71**(8), 1117 (2011).
- ²⁴Y. Brechet, J. Y. Cavaillat, E. Chabert, L. Chazeau, R. Dendievel, L. Flandin, and C. Gauthier, *Adv. Eng. Mater.* **3**(8), 571 (2001). [https://doi.org/10.1002/1527-2648\(200108\)3:8<571::AID-ADEM571>3.0.CO;2-M](https://doi.org/10.1002/1527-2648(200108)3:8<571::AID-ADEM571>3.0.CO;2-M)
- ²⁵H. W. Hatch, N. A. Mahynski, R. P. Murphy, M. A. Blanco, and V. K. Shen, *AIP Adv.* **8**(9), 095210 (2018).
- ²⁶Y. Li, H. Chen, D. Liu, W. Wang, Y. Liu, and S. Zhou, *ACS Appl. Mater. Interfaces* **7**(23), 12988 (2015).
- ²⁷K. Shanmuganathan, J. R. Capadona, S. J. Rowan, and C. Weder, *ACS Appl. Mater. Interfaces* **2**(1), 165 (2010).
- ²⁸J. R. Capadona, K. Shanmuganathan, D. J. Tyler, S. J. Rowan, and C. Weder, *Science* **319**(5868), 1370 (2008).
- ²⁹B. K. Satapathy, R. Weidisch, P. Potschke, and A. Janke, *Compos. Sci. Technol.* **67**, 867–879 (2007).
- ³⁰A. Donev, I. Cisse, D. Sachs, E. A. Variano, F. H. Stillinger, R. Connelly, S. Torquato, and P. M. Chaikin, *Science* **303**, 990–993 (2004).
- ³¹A. G. Athanassiadis, M. Z. Miskin, P. Kaplan, N. Rodenberg, S. H. Lee, J. Merritt, E. Brown, J. Amend, H. Lipson, and H. M. Jaeger, *Soft Matter* **10**, 48–59 (2014).
- ³²M. G. Basavaraj, G. G. Fuller, J. Fransaeer, and J. Vermant, *Langmuir* **22**, 6605–6612 (2006).
- ³³R. Rajamanickam, S. Kumari, D. Kumar, S. Ghosh, J. C. Kim, G. Tae, S. Sen Gupta, and G. Kumaraswamy, *Chem. Mater.* **26**(17), 5161 (2014).
- ³⁴S. Chatterjee, K. Shanmuganathan, and G. Kumaraswamy, *ACS Appl. Mater. Interfaces* **9**(51), 44864 (2017).
- ³⁵S. Chatterjee, A. Potdar, S. Kuhn, and G. Kumaraswamy, *RSC Adv.* **8**(44), 24731 (2018).
- ³⁶C. Das, S. Chatterjee, G. Kumaraswamy, and K. Krishnamoorthy, *J. Phys. Chem. C* **121**(6), 3270 (2017).
- ³⁷K. Suresh, S. Patil, P. Ramanpillai Rajamohanam, and G. Kumaraswamy, *Langmuir* **32**(44), 11623 (2016).
- ³⁸K. Suresh, D. K. Sharma, R. Chulliyil, K. D. Sarode, V. R. Kumar, A. Chowdhury, and G. Kumaraswamy, *Langmuir* **34**(15), 4603 (2018).
- ³⁹K. Suresh, A. Chowdhury, S. K. Kumar, and G. Kumaraswamy, *Macromolecules* **52**(15), 5955 (2019).
- ⁴⁰K. Suresh and G. Kumaraswamy, *J. Phys. D Appl. Phys.* **52**(21), 214002 (2019).
- ⁴¹V. R. Dugyala and M. G. Basavaraj, *Langmuir* **30**(29), 8680 (2014).
- ⁴²G. Kumaraswamy, B. Biswas, and C. K. Choudhury, *Faraday Discuss.* **186**, 61–76 (2016).
- ⁴³J. L. Bitter, Y. Yang, G. Duncan, H. Fairbrother, and M. A. Bevan, *Langmuir* **33**(36), 9034–9042 (2017).
- ⁴⁴L. Tadiello, M. D'Arienzo, B. Di Credico, T. Hanel, L. Matejka, M. Mauri, F. Morazzoni, R. Simonutti, M. Spirkova, and R. Scotti, *Soft Matter* **11**(20), 4022 (2015).
- ⁴⁵R. Scotti, L. Conzatti, M. D'Arienzo, B. Di Credico, L. Giannini, T. Hanel, P. Stagnaro, A. Susanna, L. Tadiello, and F. Morazzoni, *Polymer* **55**, 1497–1506 (2014).
- ⁴⁶T. D. Fornes and D. R. Paul, *Polymer* **44**(17), 4993 (2003).
- ⁴⁷K. Suresh, “CSIR-National Chemical Laboratory,” Ph.D. Dissertation (Pune, India, 2018).
- ⁴⁸L. J. Gibson and M. F. Ashby, *Cellular Solids: Structure and Properties* (Cambridge University Press, 1999).